Structural ordering of trapped colloids with competing interactions

L. Q. Costa Campos* and S. W. S. Apolinario†
Departamento de Física, Universidade Federal de Pernambuco, 50670-901 Recife, Pernambuco, Brazil

H. Löwen‡
Institut für Theoretische Physik II–Soft Matter, Heinrich-Heine-Universität, Düsseldorf, Universitätsstraße 1, 40225 Düsseldorf, Germany
(Received 15 August 2013; published 29 October 2013)

The structure of colloids with competing interactions which are confined in a harmonic external trap potential is analyzed numerically by energy minimization in two spatial dimensions. A wealth of different cluster structures is found to be stable including clusters with a fringed outer rim (reminiscent to an ornamental border), clusters perforated with voids, as well as clusters with a crystalline core and a disordered rim. All cluster structures occur in a two-dimensional parameter space. The structural ordering can therefore be efficiently tuned by changing few parameters only providing access to a controlled fabrication of colloidal clusters.

DOI: 10.1103/PhysRevE.88.042313 PACS number(s): 82.70.−y, 62.23.St, 68.55.−a

I. INTRODUCTION

Suspensions of mesoscopic colloidal particles are ideal model systems to study structural order and phase transitions on the fundamental length scale of the individual particles [1,2]. One key advantage of colloids is that the effective interaction between the particles can be tailored by changing the particle and solvent conditions and by putting additives into the solution. The traditional Derjaguin-Landau-Verwey-Overbeek pair interaction [3] as composed by screened electrostatic repulsion and van-der-Waals attraction provides a widely tunable range of possible pair interaction potentials which can even be augmented by adding nonadsorbing polymers leading to depletion forces [4,5]. It has been shown over the past few decades that systems with a peculiar pair potential including competing length scales may exhibit various interesting phases in the bulk including stable one-component quasicrystals [6,7], isostructural solid transitions [8–11] (see also Ref. [12]), cluster formation [13–15] (see also Refs. [16,17]), microcrystalline gels [18], microphase separation [19,20], and unusual string phases [21–23] or other exotic solid structures [24].

Colloids with competing interactions have mainly been studied in the bulk, but there are only few studies [25] where colloids with competing interactions have been explored under confinement. A key example for strong confinement is given by a parabolic external trapping potential. In fact, this is the simplest model for traps created by optical tweezers confining colloidal particles as well as for thermophoretic traps in complex plasmas. Conversely, quite a number of studies exist in the literature (see Ref. [1] for a review) for systems with simple (e.g., purely repulsive) interactions confined in a trap. As a general scenario, for sufficiently large confining strength and/or the number of trapped particles, there is a crossover to freezing within the confined cluster. For complex plasmas, this has been demonstrated for the so-called "Coulomb balls" [26–29], which are composed of crystalline shells around the potential minimum. There are "magic numbers" for which the shell structure is optimal [30,31]. A similar setup in two spatial dimensions can be realized for super-paramagnetic colloidal particles [32]. In this case the external trap can be controlled by optical tweezers leading to interesting effects like colloidal "explosions" of dense clusters when the confinement is released [33].

A few years ago, Liu *et al.* [25] studied a system with competing interactions in a parabolic trap which have consecutive repulsive-attractive-repulsive parts as a function of the interparticle distance. They find that, apart from the traditional shell structure, a formation of subclusters in the trap is possible. Even a void structure can be formed which is surrounded by a connected cluster where the void spacing is much larger than the averaged interparticle distance. The findings of Liu *et al.* [25] clearly show that the cluster structure sensitively depends on the details of the pair interaction. Therefore studies with other competing interaction forces are clearly motivated in order to get even more unexpected cluster shapes and structures.

In this paper, we consider a richer class of repulsive-attractive-repulsive pair potentials by admitting more and other parametrizations of the pair potential than in Ref. [25]. As a result, we find even more exotic cluster structures for a colloidal system confined in a parabolic trap. In detail, we predict a new cluster structure which is "fringed" at the outer boundary reminiscent to an ornamental border. The inner part of the fringed cluster can either be compact and crystalline or be perforated by voids. Moreover, we explore the crystallinity of the clusters in detail, and we find stable cluster structures which have an inner crystalline core and an outer disordered rim. The full cluster structure is obtained by extensive energy minimizations in a two-dimensional parameter space. Our theoretical predictions can be verified in real-space experiments of confined colloids with competing interactions. Control over different cluster shapes and structure by tuning only a few external parameters is highly desirable for the fabrication of optical switching elements and microsieves and filters of controlled porosity [34]. We therefore believe that our theoretical predictions are also relevant for possible applications. Moreover, we note that the finds of our work can also be relevant for hard condensed matter systems, such as in multiband superconductors, since the vortixe-vortixe interaction potential is also repulsive and

*lqcc@df.ufpe.br
†sergiowsa@df.ufpe.br
‡hlowen@thphy.uni-duesseldorf.de

attractive, respectively, at short-range and long-range distances [35–37].

This article is organized as follows: in Sec. II, we discuss our theoretical model and the computational methodology used to lower the temperature of the system, and we define some quantities that are used to characterize the structure of the clusters. In Sec. III we present our results and discussions, while the conclusions are given in Sec. IV.

II. THE MODEL

A. Interaction potential

We investigate the structural properties of a two-dimensional system composed of N monodisperse colloids confined together via an isotropic parabolic potential. The interparticle interaction potential is given by

$$U(r_{ij}) = U^{\mathrm{HC}}(r_{ij}) + U^{\mathrm{PW}}(r_{ij}) + U^{G}(r_{ij}), \tag{1}$$

where r_{ij} is the distance between the centers of the colloids i and j, $U^{\mathrm{HC}}(r_{ij})$ denotes a short range soft-core potential, $U^{\mathrm{PW}}(r_{ij})$ a midrange potential well, and $U^{G}(r_{ij})$ a shifted Gaussian-shaped potential acting at larger distances. The explicit expressions for these three parts of the potential are

$$U^{\mathrm{HC}}(r_{ij}) = \varepsilon \left(\frac{D}{r_{ij}}\right)^{m} \tag{2a}$$

$$U^{\mathrm{PW}}(r_{ij}) = -\varepsilon \exp\left[-\left(\frac{r_{ij}-D}{\alpha}\right)^{n}\right], \tag{2b}$$

$$U^{G}(r_{ij}) = R\varepsilon \exp\left[-\left(\frac{r_{ij}-\beta}{0.5D}\right)^{2}\right], \tag{2c}$$

where D defines the colloidal diameter, ε gives the strength of the potential, m and n are exponents that define, respectively, the steepness of the left and right sides of the total potential well, α is the inflection point of the term $U^{\mathrm{PW}}(r_{ij})$, while R and β are parameters used, respectively, to tune the height of the Gaussian term $U^{G}(r_{ij})$ and shift its position along the radial direction. In this work we use the value $\beta = 1.5(D+\alpha)$ in order to avoid superposition between the terms $U^{\mathrm{PW}}(r_{ij})$ and $U^{G}(r_{ij})$. Figure 1 shows a schematic representation of the interparticle interaction potential given by Eq. (1) for the particular situation of $\alpha = 1.5$ and $R = 5.1$.

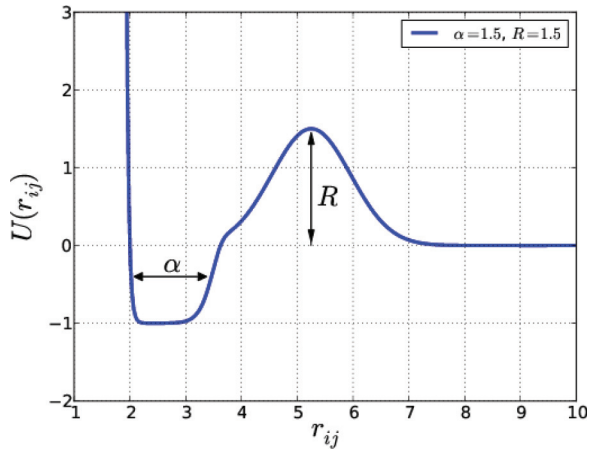

FIG. 1. (Color online) Form of the potential for the parameters $\alpha = 1.5$ and $R = 1.5$. The meaning of the parameters is indicated in the figure.

The total interaction potential used in this work, that is, Eq. (1) with Eqs. (2a)–(2c), is an extension of the potential treated in Ref. [38]. In this reference the interaction potential is given solely by the sum of the two first terms $U^{\mathrm{HC}}(r_{ij})$ and $U^{\mathrm{PW}}(r_{ij})$. It will be demonstrated, in the following sections, that the Gaussian term $U^{G}(r_{ij})$ plays a crucial role in the self-assembly process of trapped colloids and gives rise to a wide variety of configurational orders.

The external confinement potential is given by the parabolic expression

$$V(r) = \varepsilon\kappa r^{2}, \tag{3}$$

where the prefactor κ defines its relative strength. Finally, we can write the total potential energy of the system as

$$U_{\mathrm{tot}} = \sum_{i=1}^{N} V(r_i) + \sum_{i=1}^{N}\sum_{j>i}^{N} U(r_{ij}). \tag{4}$$

In order to search for stable configurations, we use a simulated annealing scheme. First, for a set of parameters, the colloids are placed randomly without superposition on a square box centered at the origin and with lateral size equal to $25D$, while the temperature is set to the value $T_0 = 5\varepsilon/k_B$. In the sequence, the temperature is slowly decreased to $T_f = 0$. The evolution of the system for a given temperature T is tracked by the overdamped Langevin equation, integrated using Euler's method, which results in the algorithm

$$\vec{r}_i(t+\Delta t) = \vec{r}_i(t) + \vec{F}_i(t)\Delta t + \vec{g}\sqrt{2k_BT\Delta t}, \tag{5}$$

where $\vec{F}_i = -\vec{\nabla}_{\vec{r}_i} U_{\mathrm{tot}}$ is the total force acting on particle i, Δt is the finite time step of the integrator, and $\vec{g}$ is a two-dimensional vector with random components, which follows a standard normal distribution of zero mean and variance one. The viscous drag coefficient is set to $\gamma = 1$. Thereby, the time scale is $t_0 = \gamma D^2/\varepsilon$.

A good convergence of the integration algorithm is achieved for $\Delta t = 10^{-5}$. For each temperature T, we iterated the system 5×10^4 time steps before decreasing the temperature by an amount of $\Delta T = 0.05$. In order to obtain statistically reliable results, the above procedure is repeated over different realizations of the random Langevin force for each set of parameters. Throughout our simulations, the following parameter values were kept constant: $m = 50$, $n = 10$, $D = 2$, $\varepsilon = 1$, and $\kappa = 0.1$, while the parameters R and α were varied.

B. Classification of the structure

1. Local structural order

In order to quickly identify different symmetries of the particle arrangements in the cluster we define the parameter $\xi_i = \frac{1}{N_i}\sum_{\{k,l\}} \sin\theta^{i}_{kl}$, where N_i is the number of first neighbors of the ith particle, $\sum_{\{k,l\}}$ runs only over those first neighbors of i that are also first neighbors of each other, and θ^{i}_{kl} are the bond angles, that is the smallest angle formed by the distance vectors $\vec{r}_{ik}$ and $\vec{r}_{il}$. An illustration of how ξ is computed is given in Fig. 2. In this example, one has $\xi_1 = (\sin\theta^{1}_{23} + \sin\theta^{1}_{34})/2$.

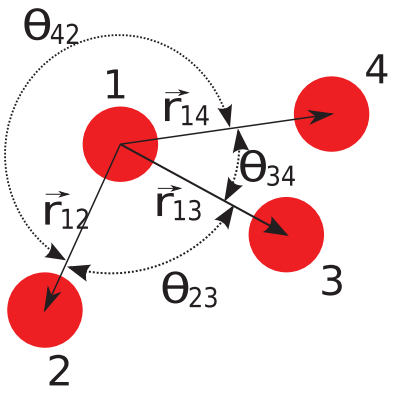

FIG. 2. (Color online) Schematic representation of a hypothetical small cluster formed by four particles, which are represented by circles and indexed by numbers from 1 to 4. θ_{kl}^{1} represents the smallest angle made by the vectors $\vec{r}_{1k}$ and $\vec{r}_{1l}$, where $k,l = 2,3$, and 4 with $k \neq l$. Only θ_{23}^{1} and θ_{34}^{1} are used in the calculation of the symmetry parameter ξ_i (see text).

The reason why we use the sine of the bond angles rather than the angles themselves is to better distinguish between, for instance, a perfectly triangular lattice from a rhombic lattice. In both cases, each particle has six neighbors forming six bond angles, so $\frac{1}{N_i}\sum_{\{k,l\}}\theta_{kl}^{i} = 360^\circ/6 = 60^\circ$ irrespective of the symmetry. However, in general, a rhombic lattice comprises two different bond angles: θ, appearing four times, and ϕ, twice. Therefore, for a rhombic lattice with, e.g., $\theta = 50^\circ$ and $\phi = 80^\circ$, $\xi_i = 0.839$, while $\xi_i = 0.866$ for the triangular lattice. In Ref. [38] it was shown that triangular, squared, and Archimedean tiling patterns can be distinguished successfully by using the symmetry parameter ξ.

Within the investigated ranges of α and R, i.e., $0.01 \leqslant \alpha \leqslant 5.5$ and $0.01 \leqslant R \leqslant 5.3$, respectively, we could identify three different local ordered phases: the triangular, squared, and an ordered mixture of square and triangular cells in a 3×2 proportion [see Fig. 5(d)], which we call mixed lattice. The values of ξ for a perfect lattice of the types triangular, squared, and mixed are, respectively, $\xi = 0.866$, 1.000, and 0.951.

2. Global structural order

The simulations performed in this work revealed that the colloids, whose dynamics is ruled by Eq. (4), can self-assemble in complex structures exhibiting interesting macroscopic patterns. A few examples of such macroscopic states are those where the cluster structures have a fringed outer boundary or an inner region that can either be compact and crystalline or be perforated by voids.

Figure 3(a) displays a typical configuration obtained through a self-assembly process for the particular case of $\alpha = 4.0$ and $R = 5.1$. We can see that such a cluster is perforated by four voids of approximately circular shape. On the contrary, for other values of these parameters, a massive core crystalline cluster becomes possible, as can be seen, for instance, in Fig. 5(a) for $\alpha = 2.8$ and $R = 0.3$.

In order to distinguish between these two types of configurations shown previously, we defined the quantity η. This latter is defined as the ratio between the quantities A_p and

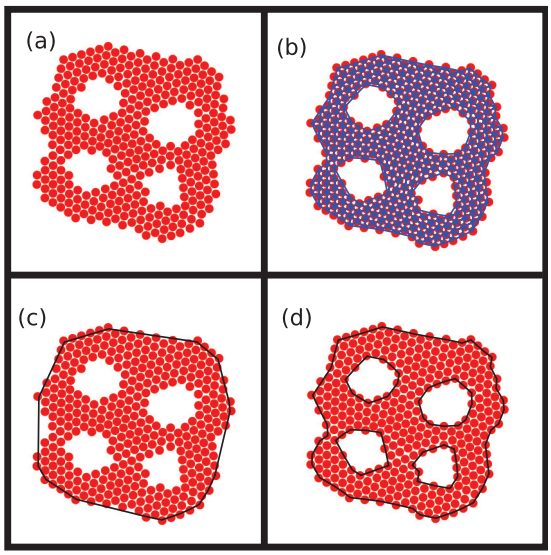

FIG. 3. (Color online) (a) Representative cluster obtained for $\alpha = 4.0$ and $R = 5.1$, and its corresponding Delaunay triangulation (b), convex hull (c), and α shapes (d).

A_c, which are, respectively, the area occupied by the colloids and the area delimited by the smallest convex polygon that contains the entire cluster, i.e., the convex hull. In calculating A_p, we first use the Delaunay triangulation to generate the set of triangles with vertices on the colloidal centers, and, second, we discard those edges of the triangles that are larger than two colloidal diameters. The total area of the remaining triangles gives the quantity A_p. An example of such triangulation can be seen in Fig. 3(b), while Fig. 3(c) shows the convex hull of such cluster. For comparison, the cluster presented in Fig. 3 has $A_p = 1122.83$, $A_c = 1552.87$, and $\eta = 0.72$, while the compact one in Fig. 5(a) has $A_p = 1202.89$, $A_c = 1232.36$, and $\eta = 0.98$.

Notice, however, that the quantity η does not allow one to unambiguously distinguish perforated clusters from the fringed ones. For instance, the fringed cluster shown in Fig. 7(a4) gives $\eta = 0.67$, which value is close to that obtained, previously, for the perforated cluster of Fig. 3, that is, $\eta = 0.72$. Yet the two clusters have rather different structures. To resolve such an issue, we can further modify the Delaunay triangulation by removing all edges that are shared between two triangles. In doing so, we obtain the cluster's α shape [39], i.e., a set of graphs representing the borders of the clusters and where each node corresponds to one particle. Figure 3(d) shows the α shape of Fig. 3(a), which comprises five different borders, that is, one external border and four internal ones.

Now, using the α shape we will define two finer-grained parameters, Ω and σ_r^2. The parameter Ω is the number of particles in the second-largest border of the cluster. This definition usually matches with the largest internal border of the cluster, as the external one is often the largest. The second parameter, σ_r^2, is the variance of the position vectors' magnitude of the particles present in the largest border, i.e., in the external concave hull. It is easy to see that the fringed clusters will have a larger value of σ_r^2 than those clusters that does not present fringes. Armed with these definitions, we are

now able to distinguish clusters with fringes from that with voids.

III. RESULTS

As expected, due to the presence of the external confinement, the self-assembled structures are constituted by only one cluster containing all particles. We found that these particles can form lattices with a well-defined microscopic ordering, such as square, mixed, and triangular lattices. Besides such a local order the self-assembled structures also possess different global patterns. For example, we found that the stable clusters can have a massive core or a core pierced by voids, while their edge can be compact, fringed, or disordered. Given this wide variety of ordering types, we made use of the quantities ξ, Ω, and σ, which were defined in the previous section, in order to obtain a more complete and quantitative description. In the next two subsections, we will investigate how the microscopic and macroscopic orderings, respectively, are influenced by the parameters R and α of the interaction potential. Note that we have divided this section into two parts only for didactic purposes; however, it is worth remembering that the same cluster has a global and local order simultaneously.

A. Local structure

In order to identify the type of local ordering present in a given cluster, the value of ξ is computed for each of the particles making up the system. With this we can know whether a given particle helps to compose some kind of lattice. For example, if the value of ξ for a given particle is within the range $0.85 \leqslant \xi_i < 0.89$, then we consider that it composes a triangular lattice. We define the quantity $\phi_{\text{triangular}}$ as the ratio between the number of particles belonging to a triangular lattice and the total number of particles. Although a particle belonging to a perfect triangular lattice has an exactly value of ξ, that is, $\xi = 0.866$, the above interval, which is used to tell whether or not a given particle belongs to a triangular lattice, shows that our results are more realistic. This last statement is based on the fact that, in experimental realizations, the self-assembled structures are usually not free of small deformations or defects.

The red region of the $R \times \alpha$ diagram [Fig. 4(a)] shows the clusters in which $\phi_{\text{triangular}} \geqslant 0.35$. In other words, such a colored area indicates the regions where at least 35% of the particles are organized in a triangular lattice. The unfilled regions of Fig. 4(a) represent the area in the phase diagram where the presence of the triangular lattice is less than 35% of the cluster or even nonexistent. Nevertheless, note that for small values of R, i.e., $R \lesssim 1.5$, the triangular lattice is always present. The latter is consistent with the fact that for small R the repulsion between the particles is not large, and hence the repulsive force cannot counterbalance the external force generated by the confinement. When the external pressure prevails, the particles organize themselves in a triangular lattice, since this type of arrangement is more compact.

We consider that a given particle belongs to a square lattice if the value of ξ for such a particle is within the range $0.98 \leqslant \xi \leqslant 1.00$. The quantity ϕ_{square} is defined as the ratio between the number of particles belonging to a triangular lattice and the total number of particles. The regions of the phase diagram $R \times \alpha$ wherein at least 35% of the particles have $\phi_{\text{square}} \geqslant 0.35$ are highlighted in green in Fig. 4(b). Notice that the unfilled region of Fig. 4(a) approximately coincides

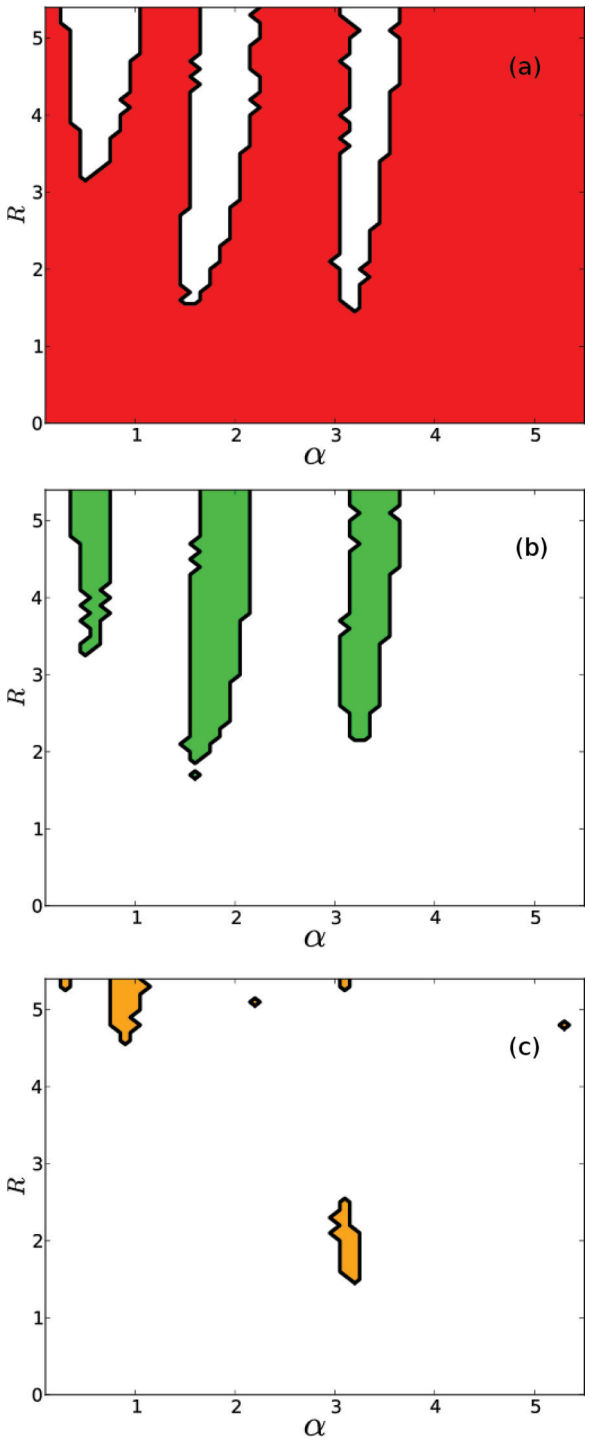

FIG. 4. (Color online) The colored regions in (a) red, (b) green, and (c) yellow indicate the areas in the phase diagram in which $\phi_{\text{triangular}}$, ϕ_{square}, and ϕ_{mixed}, respectively, are all greater than or equal to 0.35. ϕ_L is the ratio between the number of particles belonging to a lattice of the type L and the total number of particles. We have defined that a given particle belongs to a lattice of the types triangular, square, and mixed if the value of ξ to the given particle is within the ranges $0.85 \leqslant \xi_i < 0.89$, $0.98 \leqslant \xi \leqslant 1.00$, and $0.89 \leqslant \xi_i < 0.96$, respectively.

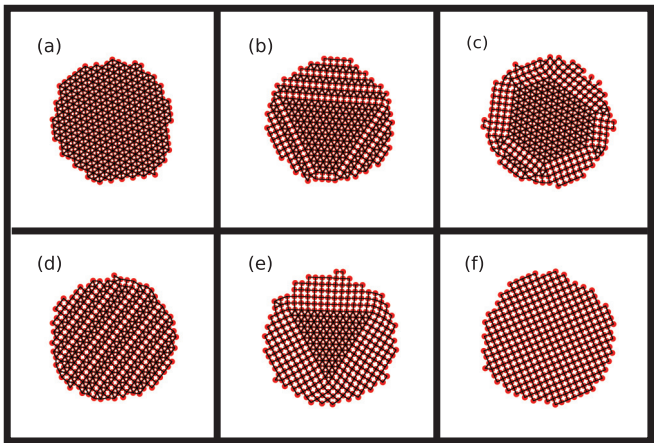

FIG. 5. (Color online) Configurations for various values of R and α. (a) $R = 0.3, \alpha = 2.8$. (b) $R = 1.3, \alpha = 3.2$. (c) $R = 1.5, \alpha = 1.6$. (d) $R = 1.5, \alpha = 3.2$. (e) $R = 2.5, \alpha = 1.8$. (f) $R = 2.5, \alpha = 3.3$.

with the region of the square lattice shown in Fig. 4(b). Anyway, it is important to note that these regions are not exactly complementary; i.e., there are regions of intersections between the red area of Fig. 4(a) and the green area of Fig. 4(b). In such intersections occur a significant presence of the square and triangular lattices, where each of these lattices has at least 35% of the total particles in the cluster.

For a perfect mixed lattice, the value of ξ for a given particle is 0.951. We consider that a given particle belongs to a mixed lattice if the value of ξ for such a particle is within the range $0.89 \leqslant \xi_i < 0.96$. The ratio between the number of particles belonging to a mixed lattice and the total number of particles is defined as ϕ_{mixed}. The mixed lattice is the one that appears less in the phase diagram, as we can see in Fig. 4(c), where the regions shaded in yellow indicate its presence. Notice that, from a simple comparison between Figs. 4(c) and 4(a), we can see that there are few regions of intersections between the triangular and mixed lattices. Nevertheless, we did not find clusters where both square and mixed lattices are present.

Typical examples of clusters found in our simulations for different values of R and α are shown in Fig. 5. Clusters formed solely by one type of lattice are shown in Figs. 5(a), 5(d), and 5(f), respectively, for the triangular, square, and mixed lattices. Heterogeneous clusters, that is, clusters formed concomitantly by two distinct types of lattices can be seen in Figs. 5(b) and 5(c). These last two configurations possess a triangular kernel surrounded, respectively, by mixed and square arrangements. As we can see, Fig. 5(e) is topologically similar to Fig. 5(c), although their triangular kernel have different geometrical shapes.

References [40,41] demonstrate that the self-assembly of colloidal particles on a quasiperiodic substrate can generate a square-triangle Archimedean tiling of the type $3^3.4^2$, that is, a tiling formed by stripes of triangles and squares with a ratio of 3 to 2. For the formation of such structures, the interaction strength between the substrate and colloids was of paramount importance. Indeed, as demonstrated by the latter two works, as the interaction between the substrate and colloids decreases, the only possible arrangement becomes the triangular one. It is worth noting that, in our model system, the formation of the square-triangle Archimedean tiling, which we named a mixed lattice, is simply due to the interaction potential between the colloidal particles. Notice that, as revealed by our previous work [38], such square-triangle Archimedean tiling can also be generated in the absence of any external confinement.

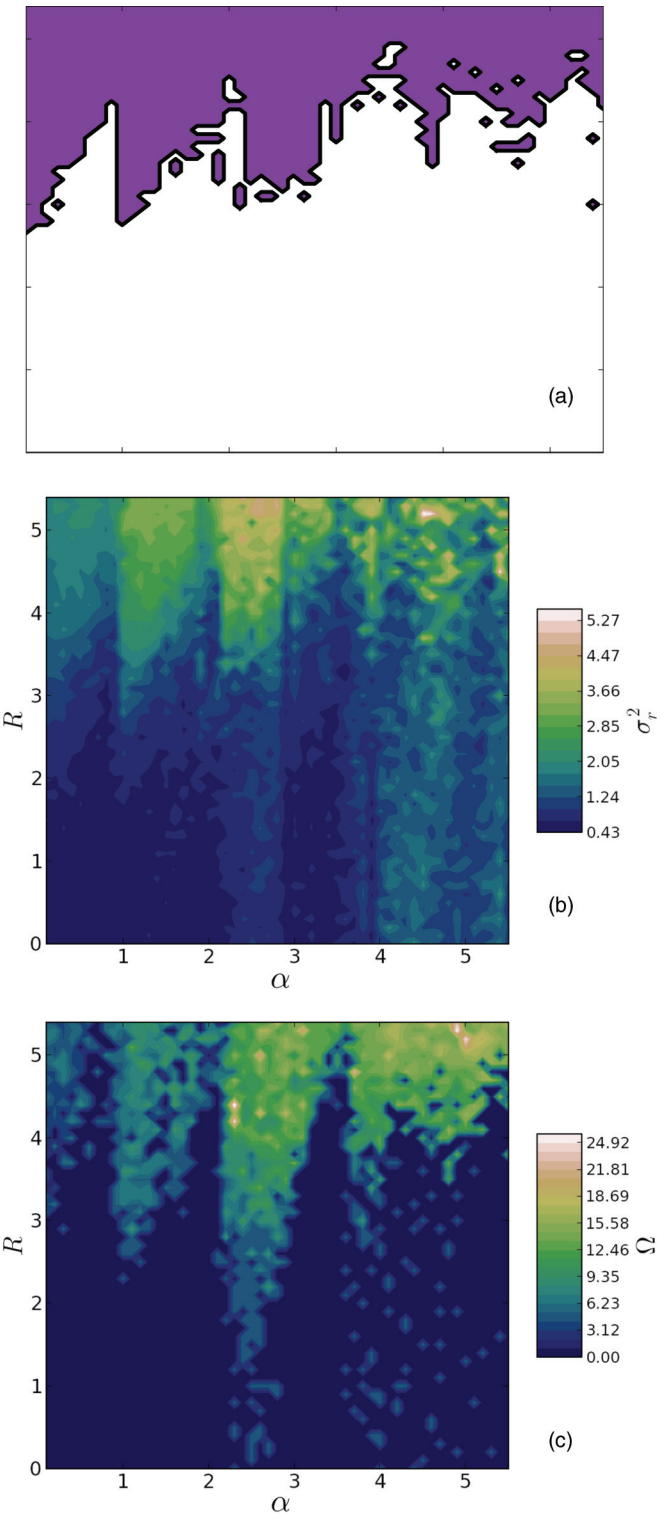

FIG. 6. (Color online) Graphic of macroscopic states. In (a) one can see the binary diagram of the results for which $\eta < 0.90$, in purple. In (b) in brown is denoted the binary diagram of perfurated clusters, i.e., the clusters on which $\Omega > 15$. In (c) σ_r^2 is shown.

B. Global cluster structure

We now turn to the global structure and focus in particular to noncompact clusters. As stated before, by definition $\eta = A_p/A_c$, where A_p is the area actually occupied by the particles while A_c is the area of the convex hull. In the case where the cluster is massive we have $\eta \simeq 1.00$, since in this situation $A_p \simeq A_p$. On the other hand, perforated and fringed clusters have values of A_p significantly lower than those of A_c, then the value of η decreases from unity. In Fig. 6(a), where the vertical and horizontal axes correspond to the magnitudes R and α, respectively, we highlight in blue the regions in which the clusters have a value of $\eta < 0.90$. We can clearly see that this occurs for high values of R; more precisely, this always occurs for $R > 4.90$.

Figure 7 shows some representative configurations of the system for several values of R and α. Note that configurations belonging to the same column have the same value α, which is given in the bottom of the figure, while the values of R, which are indicated beside each of the configurations, grow upwards. We can clearly see from Fig. 7 that in fact the configurations located near the top of the figure have decorative edges, while those for small values of R correspond to massive clusters. This result is in agreement with that obtained in Fig. 6(a).

Following from left to right the first row of Fig. 7, i.e., the row having the configurations with the highest values of R for each α, we can clearly see that the perforated clusters tend to occur for high values of α. In particular the configuration of Fig. 7(a7) exhibit three internal voids and a smooth particle radial distribution at the edge of the cluster. Furthermore, it can be seen, also from the first row of Fig. 7, that the thickness of the fringes tend to enlarge with increasing α. Notice that, for $\alpha = 0.1$ and $R = 5$ [see Fig. 7(a1)], the fringes are almost one-dimensional chains, while for $\alpha = 2.2$ and $R = 5.2$ [see Fig. 7(a4)] the thickness fringes have, approximately, three colloidal diameters. Eventually the widening of the fringes becomes sufficiently large that two neighboring fringes become able to join and form a void [see, for example, Fig. 7(a6)]. Previously, Ref. [42] has predicted the formation of a regular triangular lattice perforated by voids for two-dimensional systems of classical particles interacting via a long-range repulsive and short-range attractive potential.

The second and fourth columns of Fig. 7 demonstrate that as R grows the triangular lattice is gradually replaced by the square lattice. Moreover, such a lattice change begins by the edge of the cluster, as we can see in Figs. 7(d2) and 7(e3). At the lower limit of R, i.e., for $R = 0.0$, the total energy of the system is due only to the confinement. In such a situation,

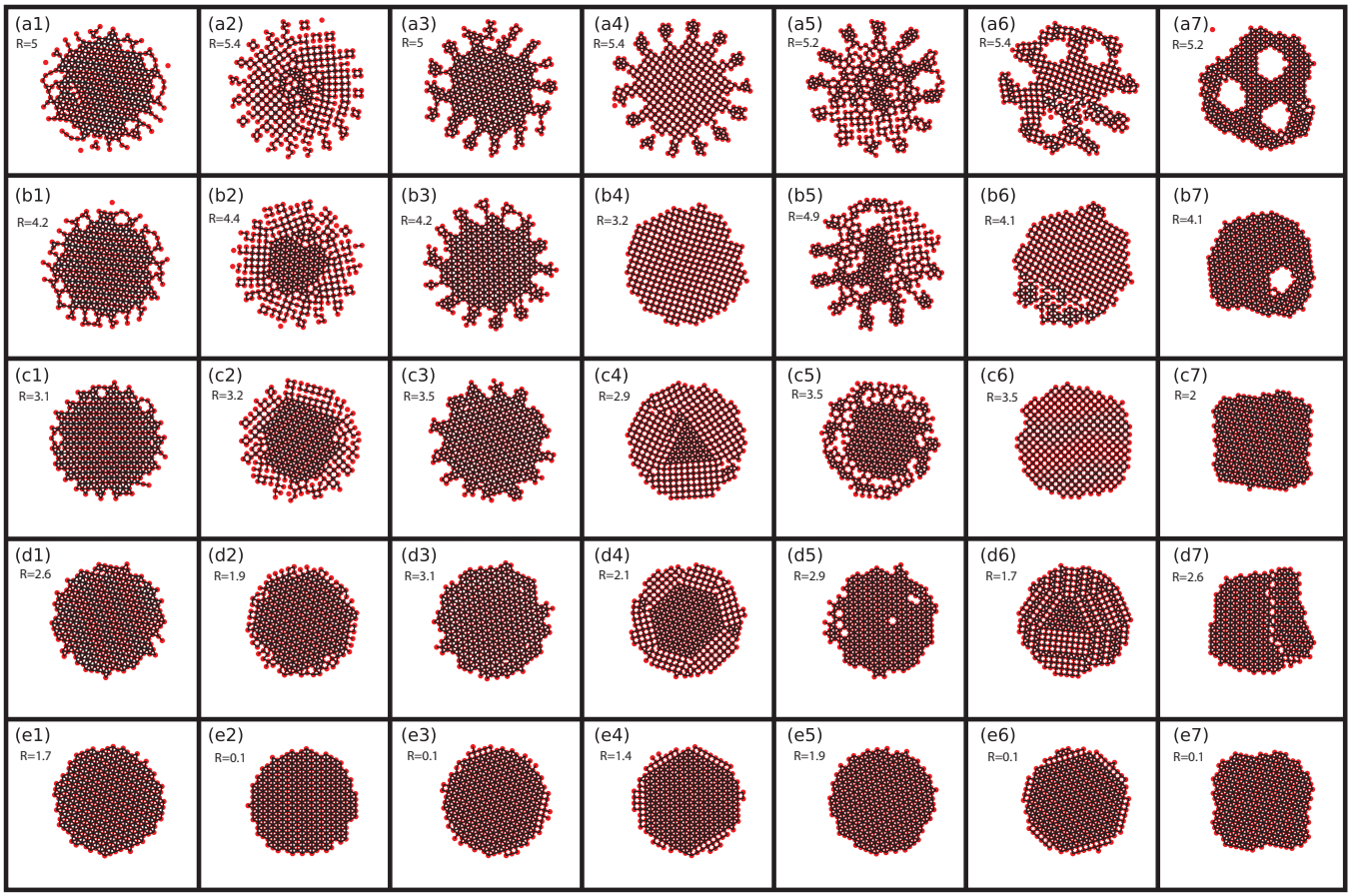

FIG. 7. (Color online) Representative configurations presented for several values of R and α. Clusters within the same column have the same value of α while the values of R grow upwards and are indicated beside each cluster. The values of R were chosen to show the greatest number of representative configurations for a given α value. From the first to the seventh column, the values of α are 0.1, 0.7, 1.4, 1.8, 2.2, 3.2, and 4.3.

the triangular lattice is the one that best minimizes the total energy, since it has the most efficient packing. On the other hand, the increase of R leads to an increase of the particles' distance, since this lowers the interaction energy. Notice that the appearance of the square lattice conforms to this latter fact, since it has larger particle spacing than that of the triangular lattice.

For increasing values of R, we also verified a delay in the formation of the fringes for clusters that can display the square or mixed lattices. This fact can be seen directly from the second and fourth columns of Fig. 7. A more quantitative result of such delay in the appearance of the fringes can be obtained from Figs. 4(a) and 6(a). Note that the first three grooves in Fig. 6(a) and the three empty regions of Fig. 4(a) occur, approximately, for the same values of α. We recall that the blanks in Fig. 4(a) correspond to regions where the square or mixed lattices can occur, as indicated by Figs. 4(b) and 4(c).

Note that a large value of Ω can indicate (1) a loop of particles near the edge of the cluster, as we see in Figs. 7(a1), 7(a5), and 7(b3) or (2) the presence of a void located closer to the center of the cluster. In the first case the system also features a large value of σ_r^2; however, for the second case, the value of σ_r^2 is not high, because as noted earlier, in such a situation the radial distribution of particles belonging to the cluster's edge is smooth, as can be seen, for instance, in Figs. 7(a1) and 7(a7). Such correspondence between the quantities σ_r^2 and Ω can be seen in Figs. 6(b) and 6(c).

Finally, we observe that, for increasing values of R, clusters with $\alpha = 1.4$ (third column of Fig. 7) evolve directly from a compact triangular structure towards a fringed cluster having a triangular core. On the other hand, in the case $\alpha = 2.2$ (fifth column of Fig. 7), we can see that as R grows the triangular lattice gives rise to a disordered arrangement near the edge of the cluster. For high values of R, i.e., $R = 5.5$ [see Fig. 7(a5)], the system achieves a fringed pattern but with a disordered core. For the case $\alpha = 3.2$ and large values of R, e.g., $R = 5.2$, the cluster can exhibit fringes and voids [see Fig. 7(a6)], whereas for small values of R, e.g., $R = 0.1$, the order of the cluster is predominantly triangular [see Fig. 7(e6)]. As we can see from Fig. 7(d6), the system can be organized into a combination of square and mixed lattices, or in a pure square lattice, as seen in Fig. 7(c6). Ultimately, for $\alpha = 4.3$ (seventh column), we can see that the triangular ordering is maintained independently from the value of R, while the macroscopic state can change from a compact [see Fig. 7(e7)] to a perforated pattern [see Fig. 7(a7)].

IV. CONCLUSION

In conclusion, we have studied confined colloids with competing pair interactions and obtained the ground state structure numerically. A wealth of stable structures is found including clusters with a fringed outer rim (reminiscent to an ornamental border), clusters perforated with voids, as well as clusters with a crystalline core and a disordered rim. Since all cluster structures occur in a two-dimensional parameter space, the structural ordering can be efficiently tuned by changing few parameters only.

For future studies it would be interesting to consider the dynamical modes ("phonons") at finite temperature [43] and the dynamical response of colloids in a time-dependent external trap [44]. The nature of the breathing mode is expected to be very different for the fringed cluster as compared to the ordinary shell structure. Moreover other types of confinement including a slit geometry [45–47] (or a cylindrical tube [48]) would be interesting to study, leading to periodic layered (or helical) structures in two (or one) dimensions.

Our results were obtained on pure energetic grounds, i.e., the temperature or any external agitation vanish. Finite temperature and agitation will melt some of the structures, but the structures are expected to stay stable for weak perturbations. For confined solids, temperature effects have been studied recently [47,49], and the influence of agitation on structure generated by competing interactions has also recently been explored [36]. The actual melting process in a finite-size cluster may depend sensitively on the details of the structures. One can surmise that the perforation voids and outermost fringes will act as natural locations where melting sets in first as temperature is increased in analogy to surface melting of solids [50,51]. All these aspects are interesting topics for further work.

ACKNOWLEDGMENTS

This work was supported by FACEPE Grants APQ-1800-1.05/12 and BIC-0503-1.05/12, SFB TR6 and the ERC Advanced Grant INTERCOCOS (Grant No. 267499).

[1] A. Ivlev, H. Löwen, G. Morfill, and C. P. Royall, *Complex Plasmas and Colloidal Dispersions: Particle-resolved Studies of Classical Liquids and Solids*, Series in Soft Condensed Matter, Vol. 5 (World Scientific, Singapore, 2012).
[2] H. Löwen, J. Phys.: Condens. Matter **13**, R415 (2001).
[3] J. P. Hansen and H. Löwen, Annu. Rev. Phys. Chem. **51**, 209 (2000).
[4] R. Roth, R. Evans, and S. Dietrich, Phys. Rev. E **62**, 5360 (2000).
[5] A. A. Louis, E. Allahyarov, H. Löwen, and R. Roth, Phys. Rev. E **65**, 061407 (2002).
[6] A. R. Denton and H. Löwen, Phys. Rev. Lett. **81**, 469 (1998).
[7] S. Fischer, A. Exner, K. Zielske, J. Perlich, S. Deloudi, W. Steurer, P. Lindner, and S. Frster, Proc. Natl. Acad. Sci. U.S.A. **108**, 1810 (2011).
[8] P. Bolhuis, M. Hagen, and D. Frenkel, Phys. Rev. E **50**, 4880 (1994).
[9] C. N. Likos, Z. T. Nemeth, and H. Löwen, J. Phys.: Condens. Matter **6**, 10965 (1994).
[10] P. Bolhuis and D. Frenkel, J. Phys.: Condens. Matter **9**, 381 (1997).
[11] A. R. Denton and H. Löwen, J. Phys.: Condens. Matter **9**, L1 (1997).

[12] D. Pini, A. Parola, and L. Reatto, J. Phys.: Condens. Matter **18**, S2305 (2006).
[13] S. Mossa, F. Sciortino, P. Tartaglia, and E. Zaccarelli, Langmuir **20**, 10756 (2004).
[14] A. Stradner, H. Sedgwick, F. Cardinaux, W. C. K. Poon, S. U. Egelhaaf, and P. Schurtenberger, Nature (London) **432**, 492 (2004).
[15] T. H. Zhang, J. Klok, H. R. Tromp, and J. Groenewold, Soft Matter **8**, 667 (2012).
[16] R. P. Sear and W. M. Gelbart, J. Chem. Phys. **110**, 4582 (1999).
[17] C. J. O. Reichhardt, C. Reichhardt, and A. R. Bishop, Eur. Phys. J. E **22**, 11 (2007).
[18] T. H. Zhang, J. Groenewold, and K. W. Kegel, Phys Chem Chem Phys **11**, 10827 (2009).
[19] A. J. Archer, Phys. Rev. E **78**, 031402 (2008).
[20] A. Ciach, Mol. Phys. **109**, 1101 (2011).
[21] G. Malescio and G. Pellicane, Phys. Rev. E **70**, 021202 (2004).
[22] G. Malescio and G. Pellicane, Nature Mater. **2**, 97 (2003).
[23] Y. Norizoe and T. Kawakatsu, J. Chem. Phys. **137**, 024904 (2012).
[24] R. D. Batten, D. A. Huse, F. H. Stillinger, and S. Torquato, Soft Matter **7**, 6194 (2011).
[25] Y. H. Liu, L. Y. Chew, and M. Y. Yu, Phys. Rev. E **78**, 066405 (2008).
[26] O. Arp, D. Block, A. Piel, and A. Melzer, Phys. Rev. Lett. **93**, 165004 (2004).
[27] O. Arp and D. Block and M. Klindworth, and A. Piel, Phys. Plasmas **12**, 122102 (2005).
[28] M. Bonitz, D. Block, O. Arp, V. Golubnychiy, H. Baumgartner, P. Ludwig, A. Piel, and A. Filinov, Phys. Rev. Lett. **96**, 075001 (2006).
[29] M. Bonitz, C. Henning, and D. Block, Rep. Prog. Phys. **73**, 066501 (2010).
[30] F. M. Peeters, V. A. Schweigert, and V. M. Bedanov, Physica B **212**, 237 (1995).
[31] S. W. S. Apolinario, B. Partoens, and F. M. Peeters, Phys. Rev. E **74**, 031107 (2006).
[32] R. Bubeck, C. Bechinger, S. Neser, and P. Leiderer, Phys. Rev. Lett. **82**, 3364 (1999).
[33] A. V. Straube, A. A. Louis, J. Baumgartl, C. Bechinger, and R. P. A. Dullens, Europhys. Lett. **94**, 48008 (2011).
[34] C. Greiser, S. Ebert, and W. A. Goedel, Langmuir **24**, 617 (2008).
[35] H. J. Zhao, V. R. Misko, and F. M. Peeters, New J. Phys. **14**, 063032 (2012).
[36] H. J. Zhao, V. R. Misko, and F. M. Peeters, Phys. Rev. E **88**, 022914 (2013).
[37] X. B. Xu, H. Fangohr, S. Y. Ding, F. Zhou, X. N. Xu, Z. H. Wang, M. Gu, D. Q. Shi, and S. X. Dou, Phys. Rev. B **83**, 014501 (2011).
[38] L. Q. Costa Campos, C. C. de Souza Silva, and S. W. S. Apolinario, Phys. Rev. E **86**, 051402 (2012).
[39] N. Akkiraju, H. Edelsbrunner, M. Facello, P. Fu, E. P. Mücke, and C. Varela, in *Proceedings of the 1st International Computational Geometry Software Workshop* (http://www.geom.uiuc.edu/software/cglist/GeomDir/shapes95def/, 1995), pp. 63–66.
[40] J. Mikhael, J. Roth, L. Helden, and C. Bechinger, Nature (London) **454**, 501 (2008).
[41] M. Schmiedeberg, J. Mikhael, S. Rausch, J. Roth, L. Helden, C. Bechinger, and H. Stark, Eur. Phys. J. E **32**, 25 (2010).
[42] C. J. Olson Reichhardt, C. Reichhardt, and A. R. Bishop, Phys. Rev. E **82**, 041502 (2010).
[43] A. Melzer, M. Klindworth, and A. Piel, Phys. Rev. Lett. **87**, 115002 (2001).
[44] M. Rex and H. Löwen, Phys. Rev. Lett. **101**, 148302 (2008).
[45] M. Schmidt and H. Löwen, Phys. Rev. Lett. **76**, 4552 (1996).
[46] E. C. Oguz, M. Marechal, F. Ramiro-Manzano, F. J. Meseguer, R. Messina, and H. Löwen, Phys. Rev. Lett. **109**, 218301 (2012).
[47] E. C. Oğuz, R. Messina, and H. Löwen, Europhys. Lett. **86**, 28002 (2009).
[48] E. C. Oğuz, R. Messina, and H. Löwen, Langmuir **94**, 28005 (2011).
[49] K. Franzrahe and P. Nielaba, Phys. Rev. E **79**, 051505 (2009).
[50] H. Löwen, T. Beier, and H. Wagner, Europhys. Lett. **9**, 791 (1989).
[51] R. Ohnesorge, H. Löwen, and H. Wagner, Phys. Rev. A **43**, 2870 (1991).